

DOI: 10.1002/cmdc.201300525

Binding Mode and Structure–Activity Relationships around Direct Inhibitors of the Nrf2–Keap1 Complex

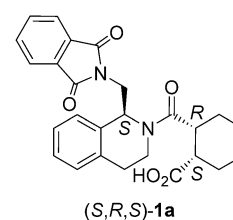
Eric Jnoff,^{*,[a]} Claudia Albrecht,^[b] John J. Barker,^[b] Oliver Barker,^[b] Edward Beaumont,^[b] Steven Bromidge,^[b] Frederick Brookfield,^[b] Mark Brooks,^[b] Christian Bubert,^[b] Tom Ceska,^[c] Vincent Corden,^[d] Graham Dawson,^[b] Stephanie Duclos,^[b] Tara Fryatt,^[b] Christophe Genicot,^[a] Emilie Jigorel,^[a] Jason Kwong,^[b] Rosemary Maghames,^[b] Innocent Mushi,^[b] Richard Pike,^[b] Zara A. Sands,^[a] Myron A. Smith,^[b] Christopher C. Stimson,^[b] and Jean-Philippe Courade^[a]

An X-ray crystal structure of Kelch-like ECH-associated protein (Keap1) co-crystallised with (1*S*,2*R*)-2-[(1*S*)-1-[(1,3-dioxo-2,3-dihydro-1*H*-isoindol-2-yl)methyl]-1,2,3,4-tetrahydroisoquinolin-2-carbonyl]cyclohexane-1-carboxylic acid (compound (*S,R,S*)-**1a**) was obtained. This X-ray crystal structure provides breakthrough experimental evidence for the true binding mode of the hit compound (*S,R,S*)-**1a**, as the ligand orientation was found to differ from that of the initial docking model, which was available at the start of the project. Crystallographic elucidation of this binding mode helped to focus and drive the drug design process more effectively and efficiently.

Neurodegenerative diseases are conditions with high unmet medical needs for patients, and currently available treatments only provide symptomatic relief. In recent years, nuclear factor erythroid 2-related factor 2 (Nrf2) has become an attractive neuroprotective target, as the Nrf2 pathway represents a natural cell defense mechanism.^[1] Nrf2 is a transcription factor and member of the Cap'N'collar family of proteins.^[2] It regulates the antioxidant response element (ARE)-mediated transcription of a myriad of antioxidant and protective genes to counteract the harmful effects of reactive oxygen species or xenobiotic damage.^[3–6] Under basal conditions, Nrf2 is tightly regulated in the cytoplasm by Kelch-like ECH-associated protein (Keap1) and is targeted for ubiquitin-mediated proteasomal degrada-

tion, which maintains low levels of Nrf2 protein. Upon oxidative stress, Nrf2 dissociates from Keap1 and translocates into the nucleus, where it forms heterodimers with a variety of transcriptional regulatory proteins.^[7] These protein complexes then associate with the ARE to induce gene transcription of cytoprotective enzymes to prevent toxicity. A number of articles have described the exciting preclinical neuroprotective effects of Nrf2 not only in Parkinson's^[8–10] and Alzheimer's disease,^[11,12] but also in multiple sclerosis^[13] and amyotrophic lateral sclerosis.^[14] Moreover, our research group recently reported the importance of Nrf2 in epilepsy;^[15] we demonstrated that Nrf2 mRNA is significantly increased in human epileptic hippocampal tissue. Additionally, Nrf2 and the expression levels of its downstream genes [heme oxygenase 1 (HO-1), NAD(P)H quinone oxidoreductase 1 (NQO1), glutathione S-transferases (GSTs)] increased progressively in a spontaneously occurring seizure model of epilepsy in mice. Importantly, mice that over-express Nrf2 displayed fewer seizures with a profound decrease in microglia activation and preservation of hippocampal neurons. Almost all known ARE activators behave as indirect inhibitors of the Nrf2–Keap1 interaction; they are believed to disrupt this protein–protein interaction by oxidation or covalent modification of cysteine residues on Keap1, thus releasing Nrf2.^[16]

Very recently, Hu et al.^[17,18] described (*S,R,S*)-**1a** as the first cysteine-independent activator of Nrf2 to act as a direct inhibitor of Nrf2–Keap1 complex formation. This single diastereomer, containing three chiral centers, originated from a mixture of diastereomers of **1a**, which was identified as a hit from a high-throughput screen of the NIH MLPCN library of small molecules. Prior to this publication, we had independently mined the NIH screening data, which was in the public domain, and selected **1a** as worthy of confirmation and deconvolution. Subsequent preparation and biological evaluation of each pure stereoisomer confirmed that the most active compound is (*S,R,S*)-**1a**. Herein we describe how structural biology informed our understanding of the binding pose, which in turn helped to drive the drug design process.



[a] Dr. E. Jnoff, Dr. C. Genicot, Dr. E. Jigorel, Dr. Z. A. Sands, Dr. J.-P. Courade
UCB Pharma, UCB NewMedicines
Chemin du Foriest, 1420 Braine-l'Alleud (Belgium)
E-mail: eric.jnoff@ucb.com

[b] Dr. C. Albrecht, Dr. J. J. Barker, Dr. O. Barker, Dr. E. Beaumont,
Dr. S. Bromidge, Dr. F. Brookfield, Dr. M. Brooks, Dr. C. Bubert,
Dr. G. Dawson, Dr. S. Duclos, Dr. T. Fryatt, Dr. J. Kwong, R. Maghames,
I. Mushi, Dr. R. Pike, Dr. M. A. Smith, Dr. C. C. Stimson
Evotec, 114 Innovation Drive, Milton Park
Abingdon, Oxfordshire OX14 4RZ (UK)

[c] Dr. T. Ceska
UCB Pharma, UCB NewMedicines
208 Bath Road, Slough, Berkshire SL1 3WE (UK)

[d] V. Corden
CEM Microwave Technology Ltd.
2 Middle Slade, Buckingham, Buckinghamshire MK18 1WA (UK)

Supporting information for this article is available on the WWW under
<http://dx.doi.org/10.1002/cmdc.201300525>.

Compound (*S,R,S*)-**1a** was docked into two crystal structures of the human Keap1 Kelch domain, PDB ID: 2FLU (co-crystal structure with Nrf2 fragment)^[19] and PDB ID: 1ZGK (apo structure),^[20] as these structures showed differing conformations for Arg380 and Arg415. Visual inspection of the docked poses and comparison of the intermolecular protein–ligand interactions revealed that the top-ranked pose in 2FLU mimics several interactions observed between Keap1 and Nrf2. Interestingly, our top pose posits the cyclohexyl group of (*S,R,S*)-**1a** in a similar pocket to the exemplary docked pose published by Hu and co-workers,^[17] with the remainder of the molecule forming quite different interaction patterns. In particular, our solution allowed the acid to form both a salt bridge with Arg415 and a hydrogen bond with Ser508, in a similar manner to one of the Nrf2 acidic moieties. In addition to these Nrf2-like interactions, the cyclohexane ring, which adopts a conformation with the larger amide substituent positioned equatorially, makes a hydrophobic contact with Tyr525 (not shown), and the carbonyl group of the amide linker between the tetrahydroisoquinoline (THIQ) moiety and the cyclohexane ring interacts with Ser555. The THIQ group interacts with Tyr572 (π -stacking) and the six-membered ring of the phthalimide moiety forms a hydrophobic contact with Tyr334. Finally, one of the phthalimide carbonyl groups interacts by a hydrogen bond with Arg415 (Figure 1 a).

While this pose appeared promising, the eventual co-crystal structure revealed a very different mode of binding (PDB ID: 4L7B).^[21] In the presence of ligand **1a**, we found that the Arg415 side chain adopts a conformation different from that observed in the Nrf2-bound Keap1 structure (PDB ID: 2FLU) used for the initial docking efforts pose. Surprisingly, the cyclohexane ring observed in the Keap1–**1a** co-crystal structure adopts an unusual conformation, with the larger amide substituent positioned axially. The top-ranked docked pose for the 1ZGK structure (data not shown) was significantly closer to the crystallographically observed binding mode, but was initially less favored, as the interactions with Keap1 appeared less Nrf2-like.

Initial attempts at obtaining ligand complexes with (*S,R,S*)-**1a** using the published mouse and human Keap1 Kelch domain crystal structures were unsuccessful due to occlusion of the Nrf2 binding site in the crystal lattice by loop residues. A panel of rationally designed mutants were explored to create a system with different crystal packing that would be amenable to co-crystallisation or soaking with small molecules. The human Keap1 Kelch domain (321–609) with the R354D point mutation and the histidine tag relocated to the C terminus of the construct subsequently co-crystallised with (*S,R,S*)-**1a** (Figure 1 b).

The conformation of (*S,R,S*)-**1a** in the crystal structure shows the aromatic ring of the THIQ group further into the central pore, and the cyclohexane carboxylic acid/phthalimide moieties extending outward, making interactions with Tyr572, Ser602, Arg415, and Asn414. Compared with the apo structure (PDB ID: 1ZGK) both Arg380 and Arg415 side chains are re-orientated away from the central pore closer to the proteinaceous aspect of the protein, in order to accommodate

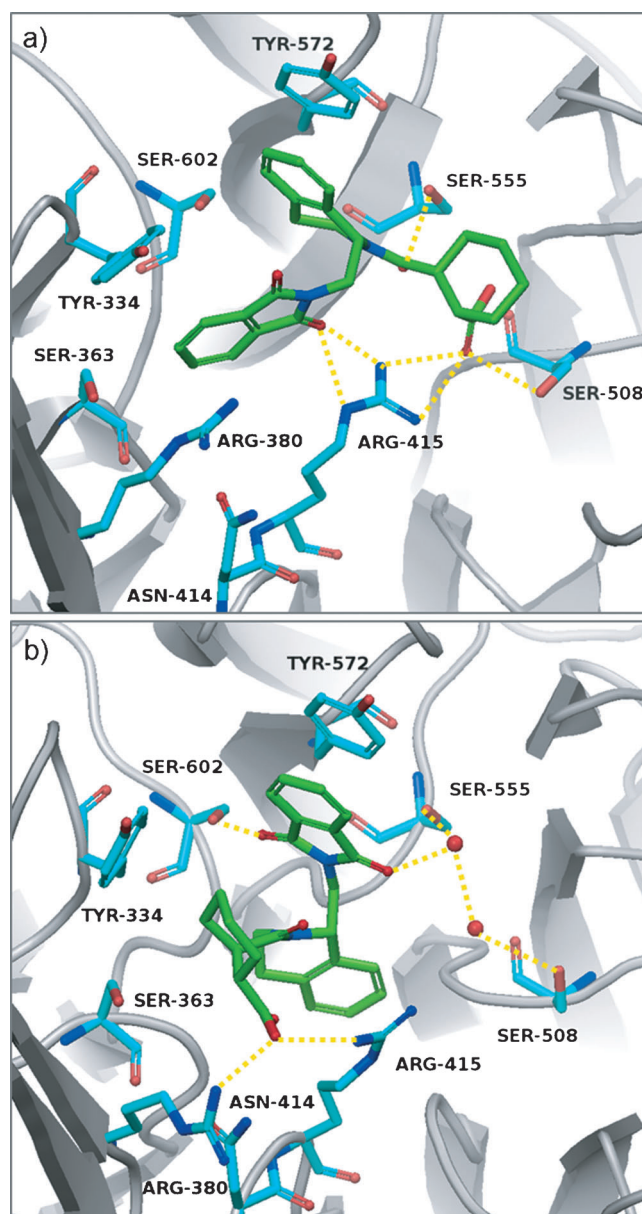


Figure 1. a) Docking pose and b) co-crystal structure of (*S,R,S*)-**1a** with Keap1.

(*S,R,S*)-**1a**. The carboxylic acid group fits into a groove formed by Arg415, which extends into the center of the pore, and Asn414 with hydrogen bonds to both residues. Arg415 is itself positioned between the acid and the carbonyl group that links the THIQ moiety to the cyclohexane ring. The phthalimide carbonyl group is hydrogen bonded to Ser602, and the phenyl ring forms a face-to-face π -stack with Tyr572.

Finally, there also appears to be a water-mediated hydrogen bond between the second phthalimide carbonyl oxygen atom and Ser555. The binding pocket of Keap1 that accommodates (*S,R,S*)-**1a** is the one used by the Nrf2 peptide and has recently been involved with other small molecules co-crystallised with Keap1.^[22] As mentioned above, the THIQ moiety sits at the top of the central pore, suggesting some potential chemical space

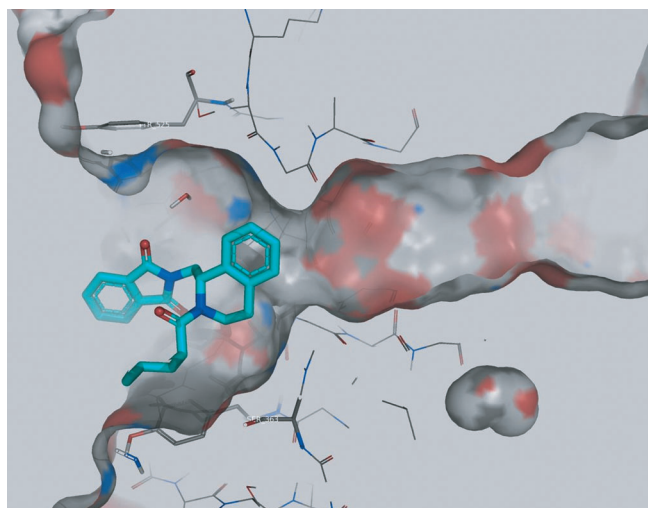
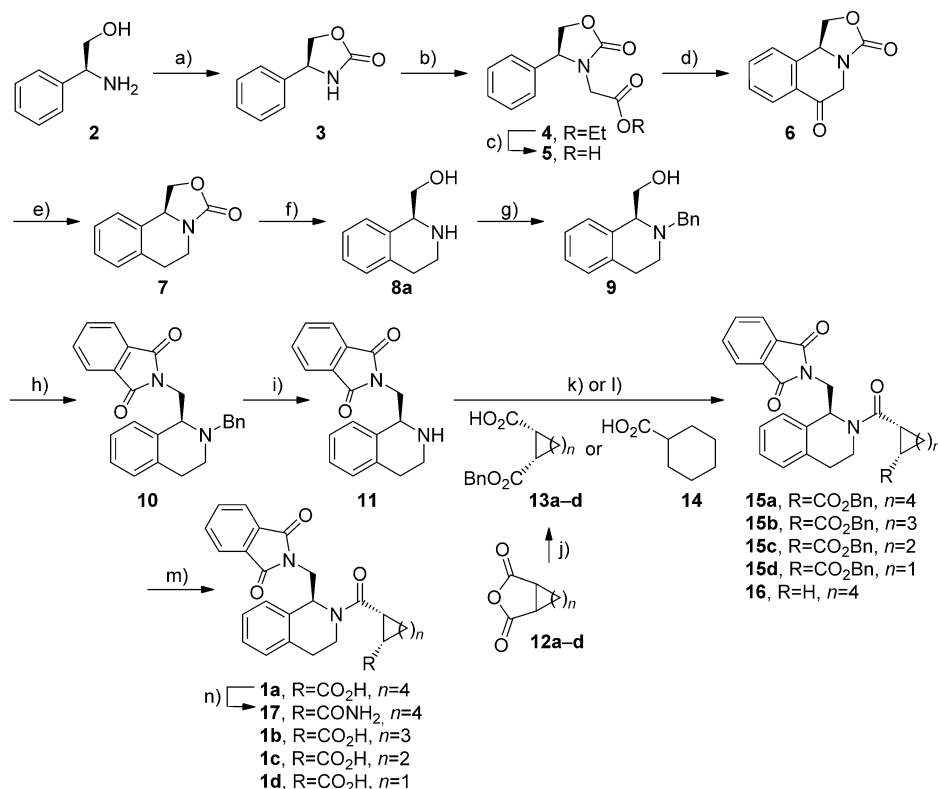


Figure 2. Extension from the THIQ into the central channel.

available around the aromatic ring for incorporating new interactions to increase affinity toward Keap1 (Figure 2).

Optically pure THIQ **1 a** was prepared as shown in Scheme 1. Treatment of (*S*)-phenylglycinol **2** with triphosgene gave the cyclic carbamate **3**, which was subsequently alkylated with ethyl bromoacetate to give compound **4**. Saponification and



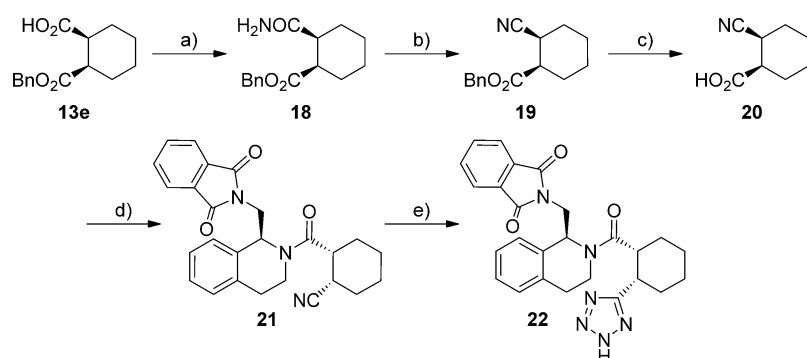
Scheme 1. Reagents and conditions: a) triphosgene, CH₂Cl₂, TEA, 0 °C; b) ethyl bromoacetate, K₂CO₃, DMF; c) NaOH, THF, H₂O; d) thionyl chloride, CH₂Cl₂ then AlCl₃, 0 °C; e) H₂, Pd/C, EtOH; f) NaOH, EtOH, reflux; g) benzyl bromide, DIPEA, THF; h) DIAD, PPh₃, THF, phthalimide; i) H₂, Pd/C, EtOH; j) quinidine, benzyl alcohol, toluene, −55 °C, 96 h; k) T3P, **13 a–d**, CH₂Cl₂, TEA; l) cyclohexane carbonyl chloride, pyridine, CH₂Cl₂; m) H₂, Pd/C, THF, EtOAc, EtOH; n) (COCl)₂, CH₂Cl₂, NH₃(g).

subsequent Friedel–Crafts acylation provided tetrahydroquinolone **6**, which was reduced to afford **7**. The cyclic carbamate **7** was cleaved to provide (*S*)-1-hydroxymethyl THIQ **8 a**; following selective benzylation of the nitrogen atom, the phthalimide group was installed by Mitsunobu reaction under standard conditions. The *N*-benzyl group was cleaved by hydrogenolysis, and coupling with the optically pure (*1R,2S*)-cyclohexane-1,2-dicarboxylic acid monobenzyl ester **13 a** yielded, after hydrogenolysis of the benzyl group, compound (*S,R,S*)-**1 a**. A range of optically pure cyclic mono-protected diacid moieties, **13 a–d**, were prepared from **12 a–d** according to the published procedure,^[23] in which the corresponding *cis*-cyclic anhydrides were desymmetrised by quinidine-mediated stereoselective ring opening. Coupling reaction of **13 b–d** or **14** with THIQ **11** yielded the five-, four-, and three-membered ring analogues **1 b–d** and the des-acid compound **16**, respectively. Conversion of **1 a** into the corresponding primary amide **17** was carried out under standard conditions (Scheme 1).

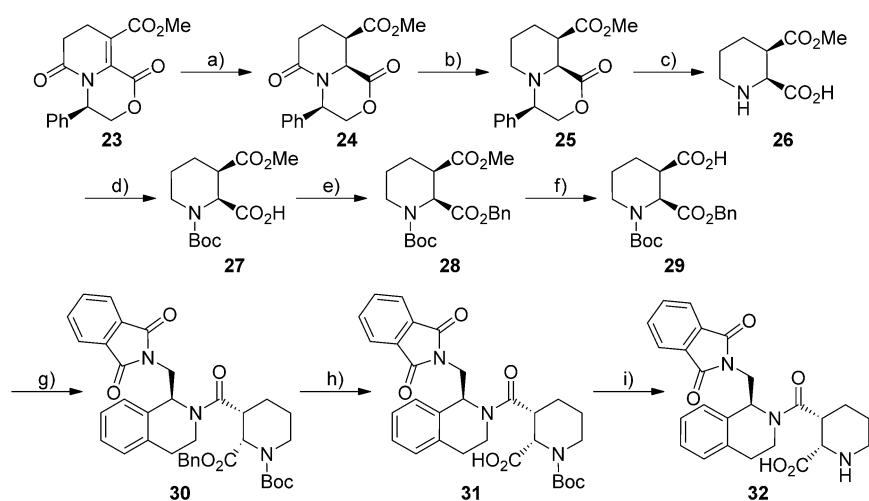
Tetrazole analogue **22** was prepared by coupling THIQ **11** with (*1R,2S*)-2-cyanocyclohexanecarboxylic acid **20** followed by conversion of the cyanide moiety into the tetrazole group. Compound **20** was prepared in three steps by starting from **13 e**, which was obtained in a similar manner to **13 a** but by using quinine rather than quinidine as chiral catalyst in order to obtain the opposite enantiomer (Scheme 2).

Amino acid **32** was prepared by coupling *N*-protected piperidine **29** and THIQ **11** followed by two deprotection steps. Synthesis of the optically pure piperidine **29** was performed according to a published procedure^[24] by starting from (*R*)-phenylglycinol, and conversion toward piperidine **32** was performed as depicted in Scheme 3.

Access to various substituted THIQ structures was achieved by a modification of the initial Mitsunobu reaction. Formation of the cyclic sulfamates **33 a,b** was carried out by reaction of the corresponding 1-hydroxymethyl THIQ **8 a** and **8 b** with thionyl chloride, followed by oxidation using ruthenium trichloride/sodium periodate. The ring-opening step was performed with a wide range of nucleophiles, including phenyl magnesium bromide, pyridone, and the anions of amides. Subsequent coupling of the respective THIQs **34–38** with **13 a** afforded, after hydrogenolysis, the fully elaborated compounds **40, 43, 44, 46, and 48** (Scheme 4).



Scheme 2. Reagents and conditions: a) $(\text{COCl})_2$, NH_3 , CH_2Cl_2 ; b) SOCl_2 , MeCN ; c) BBr_3 , CH_2Cl_2 , -78°C ; d) SOCl_2 then **11**, pyridine; e) Bu_3SnN_3 , xylene, 140°C .



Scheme 3. Reagents and conditions: a) Pd/C , H_2 , MeOH ; b) BH_3 , DMS , THF ; c) $\text{Pd}(\text{OH})_2/\text{C}$, H_2 , MeOH ; d) Boc_2O , NaHCO_3 , dioxane; e) BnBr , DBU , CH_2Cl_2 ; f) LiOH , THF ; g) **11**, HATU , DIPEA , DMF ; h) H_2 , Pd/C , MeOH ; i) HCl , Et_2O .

Starting from the THIQ intermediate **9**, access to the succinimide **52** was achieved using the same synthetic route as for compound **1a**. Thus, coupling of succinimide with the hydroxy-THIQ under Mitsunobu conditions provided the fully protected intermediate **49**. Debenzylation, coupling with acid **13a**, and final deprotection of the benzyl ester provided the succinimide **52** as shown in Scheme 5.

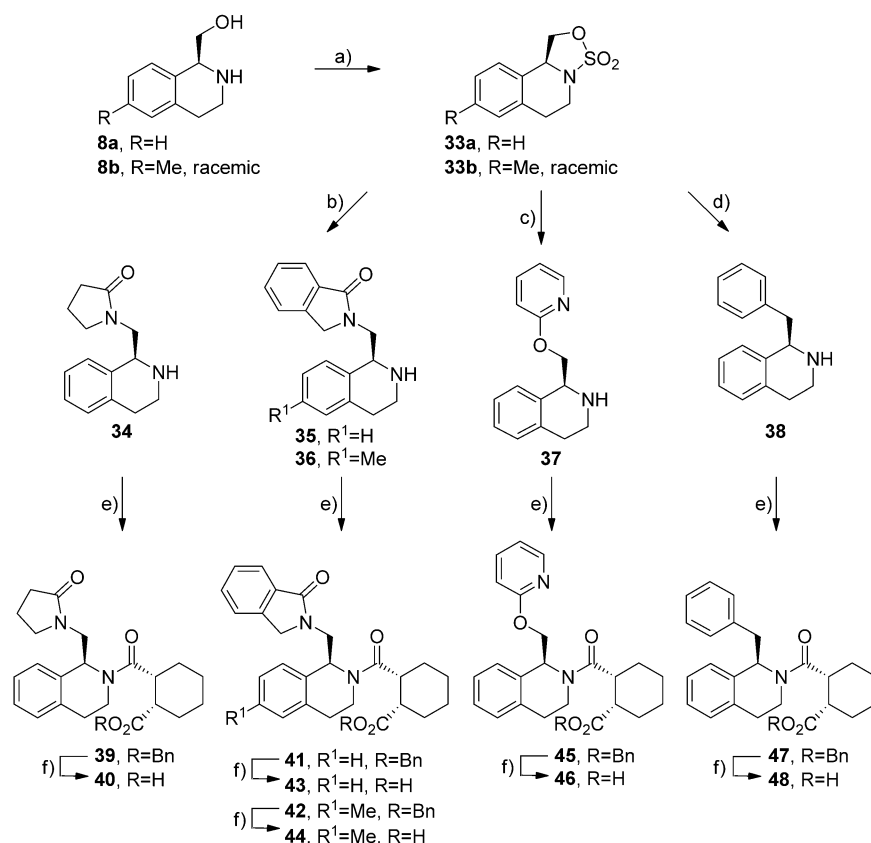
While introduction of a methyl group at position 6 of the THIQ moiety (in **44**) was readily performed as outlined in Scheme 4 by starting from (*S*)-2-amino-2-*para*-tolylethanol, an alternative pathway was followed to prepare the isomer **59**. Acylation of 2-*ortho*-tolylethylamine **53** and subsequent Bischler–Napieralski reaction allowed the synthesis of 3,4-dihydroisoquinoline **55**. Introduction of the isoxindole moiety by nucleophilic substitution, reduction of the imine group, and HATU-mediated coupling of the resulting THIQ **57** with **13a** yielded compound **58** as a pair of diastereomers, which were readily separated by column chromatography. Hydrogenolysis of the benzyl group provided the optically pure 5-methyl-substituted derivative **59** (Scheme 6).

Disruption of the Nrf2–Keap1 protein–protein complex was measured by fluorescence polarisation assay using Keap1 Kelch domain/Nrf2-ETGE peptide and is expressed as IC_{50} values (Table 1). Under these assay conditions, the initial starting hit **1a** displayed an IC_{50} value of $2.3\ \mu\text{M}$. The pendent phthalimide moiety linked to the central THIQ core is well known to be a potential problem with respect to the developability of molecules, so our initial task was to carry out investigations to determine whether this group could be replaced. Interestingly, isoxindole **43** retained a good level of potency (IC_{50} : $1.1\ \mu\text{M}$) despite the absence of one hydrogen bond acceptor group. The X-ray co-crystal structure displayed interactions between the carbonyl group of the isoxindole and Ser602 in addition to a putative π – π stacking of the aromatic ring with Tyr572 (PDB ID: 4N1B;^[25] Figure 3a). We were surprised to discover that succinimide **52** retained potency (IC_{50} : $2\ \mu\text{M}$) and that removal of a further carbonyl group, as shown with pyrrolidinone **40**, retained activity (IC_{50} : $1.2\ \mu\text{M}$).

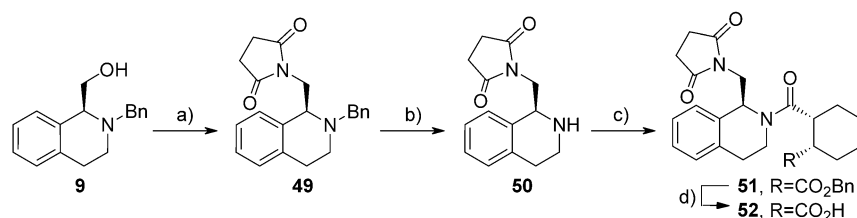
These results indicate that either the π – π interaction does not provide significant binding energy, or that the desolvation penalty incurred by placing a lipophilic group in a solvent-exposed area of the protein negates any positive binding energy from the π -stacking interaction. On the other hand, complete removal of the hydrogen bond acceptors whilst keeping the

| Table 1. Affinity of compounds for the Keap1 Kelch domain. | | | |
|--|---|-----------|---|
| Compd | IC_{50} [μM] ^[a] | Compd | IC_{50} [μM] ^[a] |
| 1a | 2.3 ± 0.06 | 32 | 69.7 ± 9.95 ^[b] |
| 1b | 2.2 ± 0.44 | 40 | 1.2 ± 0.14 |
| 1c | 8.0 ± 0.09 | 43 | 1.1 ± 0.19 |
| 1d | 20.8 ± 3.79 | 44 | 7.1 ± 0.51 |
| 16 | > 100 | 46 | > 100 |
| 17 | > 100 | 48 | > 100 ^[c] |
| 21 | > 100 | 52 | 2.0 ± 0.38 |
| 22 | 7.4 ± 0.89 | 59 | 0.75 ± 0.32 |

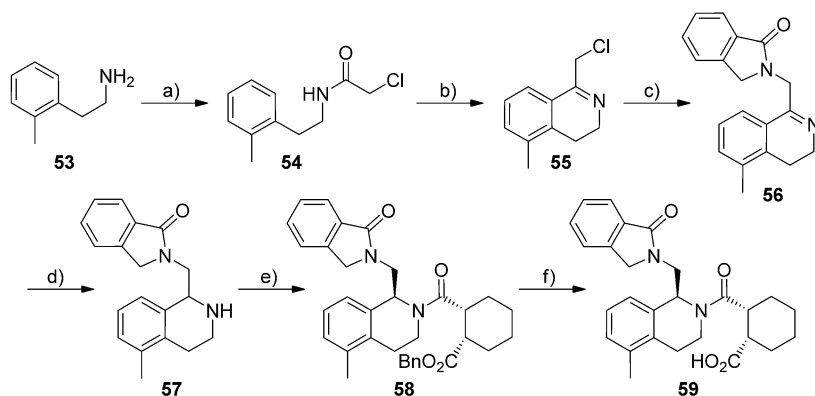
[a] IC_{50} values determined by FP assay, and are the means \pm SEM ($n = 3$ – 5); active compounds inhibit with 80–100% control relative to the Nrf2 reference peptide. [b] Inhibition with 60% control. [c] 30% inhibition at $100\ \mu\text{M}$.



Scheme 4. Reagents and conditions: a) SOCl_2 , imidazole, TEA, CH_2Cl_2 , 0°C then $\text{RuCl}_3/\text{NaIO}_4$, $\text{EtOAc}/\text{H}_2\text{O}$, 0°C ; b) NaH, THF, isoxindole or pyrrolidone; c) 2-pyridone, Cs_2CO_3 , THF, 0°C ; d) PhMgBr , THF, 0°C ; e) **13a**, SOCl_2 then pyridine or HATU, DIPEA, DMF; f) H_2 , Pd/C, EtOH.



Scheme 5. Reagents and conditions: a) succinimide, DIAD, PPh_3 , THF; b) H_2 , Pd/C, EtOH; c) **13a**, EDC, TEA, DMAP, CH_2Cl_2 ; d) H_2 , Pd/C, EtOH



Scheme 6. Reagents and conditions: a) ClCH_2COCl , K_2CO_3 , CH_2Cl_2 ; b) P_2O_5 , xylenes; c) isoxindole, Cs_2CO_3 , DMF; d) NaBH_4 , MeOH; e) **13a**, HATU, DIPEA, DMF; f) H_2 , Pd/C, THF/ H_2O .

putative interaction with Tyr572 significantly decreases activity, as shown with compound **48**, which displayed only 30% inhibition at $100\ \mu\text{M}$. The pyridyl ether **46**, which was expected to place a hydrogen bond acceptor in the correct region of space, lost all measurable activity. It is likely that the very specific directionality of the available lone pair of the pyridine ring does not allow the necessary hydrogen bond to form.

An investigation around the saturated ring bearing the acid function revealed that the cyclopentyl analogue **1b** is essentially equipotent to the cyclohexyl derivative **1a**, while potency decreased progressively for the four- and three-membered ring compounds **1c** and **1d**. Introduction of nitrogen atom into the six-membered ring, leading to piperidine analogues, was investigated. Among the various isomers, only the α -amino acid **32** was found to be active, but with a significant decrease in potency (IC_{50} : $69.7\ \mu\text{M}$). As the activity of this compound class is expected to occur in the brain, modulation of the carboxylic acid moiety was a key goal; it was hoped that this would help enable adequate levels of brain exposure. However, neither removal of the carboxylic acid function (in **16**) nor its replacement by carboxamide (**17**) or nitrile (**21**) yielded active compounds. Only replacement of the acid function with a tetrazole group (compound **22**) was acceptable, leading to a small decrease in potency (IC_{50} : $7.4\ \mu\text{M}$). The crystal structure of this tetrazole compound **22** bound to Keap1 showed an analogous pose to that of **1a**. However, although the tetrazole moiety packs between Arg380 and Arg415, a different hydrogen bonding pattern is observed (PDB ID: 4L7C;^[26] Figure 3b).

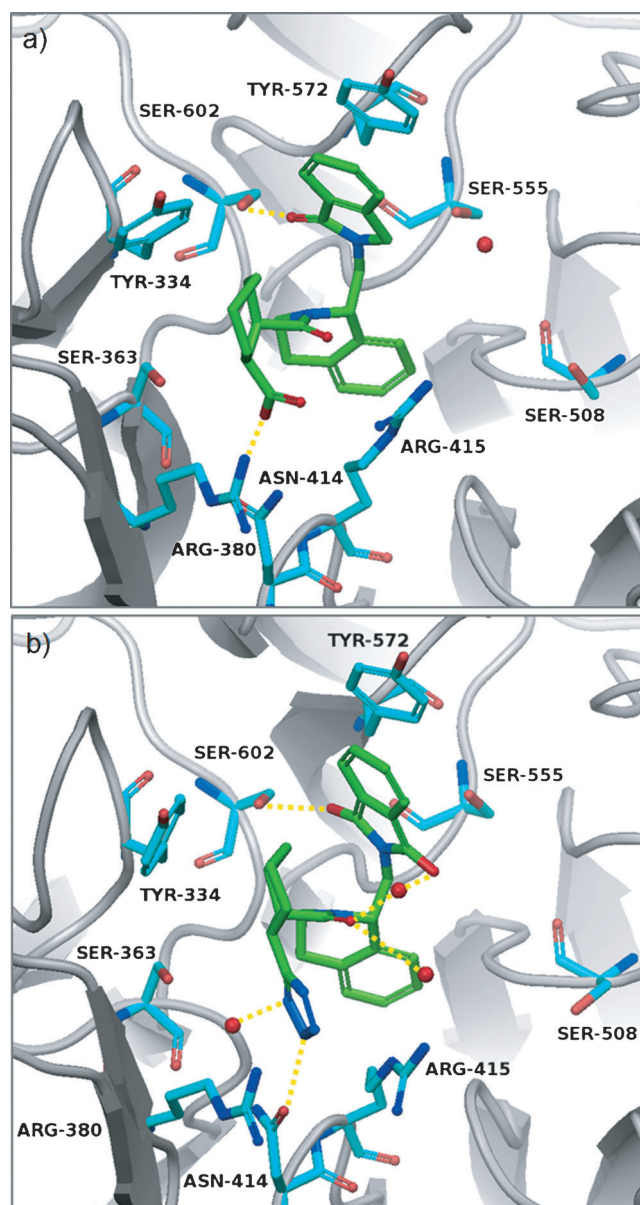


Figure 3. Co-crystal structures of Keap1 with compounds a) 43 and b) 22.

As mentioned above, the crystal structure places the phenyl ring of the THIQ on top of the central pore of the Kelch domain and appears to show potential for extending groups into the pore, thus opening up two possibilities for further exploration: The first was to nestle a lipophilic group into the opening, taking advantage of van der Waals interactions and a good shape fit to increase potency. The second possibility was to extend a portion of the molecule into the pore, thereby affording us an opportunity to create hydrogen bond interactions with a number of backbone carbonyl groups, or to displace or interact with water molecules observed inside the pore. Methylation of the 6-position of the THIQ leading to **44** was tolerated, but not optimal relative to a methyl group at the 5-position, providing ligand **59** (PDB ID: 4L7D),^[27] which showed increased potency (IC_{50} : 0.75 μM). This result suggests a good shape fit of the molecule toward the pore where the

methyl group likely acts as a lipophilic “plug”, giving a moderate boost in potency over the original hit **1a**. Further modifications that target that area of the molecule are currently under investigation.

In addition to an exploration of structure–activity relationships, assessment of in vivo brain exposure was performed. Acid compound **1a** was restricted to the peripheral compartment in mice (unbound brain-to-plasma (B_u/P_u) ratio < 0.01), being a P-glycoprotein (P-gp) substrate, as predicted by a high efflux ratio (ER value of 20) observed in an MDCK-MDR1 assay. The efflux was mitigated by using Mdr1a/1b/Bcrp knock-out mice, in which **1a** did achieve an improved level of free brain exposure (0.18 μM) and a much better B_u/P_u ratio (0.4), confirming the P-gp substrate property of **1a**. This B_u/P_u ratio is very similar to the biologically inactive non-acid compound **16** administered in wild-type mice, but with lower free brain exposure. Neither replacement of the carboxylic acid group by the tetrazole bioisostere **22** nor the zwitterionic amino acid **32** displayed improved profiles over that of **1a** (Table 2). Despite the

| Table 2. Physicochemical and DMPK properties. | | | | | |
|---|---------------|---------------------------------------|-------------------|------------------------------|--|
| Compd | Log $D^{[a]}$ | PSA [\AA^2] ^[b] | ER ^[c] | B_u/P_u ^[d] | C_u [μM] ^[e] |
| 1a | 1.36 | 95 | 20 | < 0.01 0.4 ^[f] | < 0.01 0.18 ^[f] |
| 16 | 3.59 | 58 | 0.7 | 0.3 | 0.003 |
| 22 | 1.15 | 112 | 28 | NT ^[g] | NT ^[g] |
| 32 | 0.69 | 107 | NT ^[g] | < 0.01 | < 0.01 |
| 43 | 1.11 | 78 | 7.5 | NT ^[g] | NT ^[g] |
| 48 | 2.06 | 58 | 0.7 | 0.9 | 0.2 |

[a] Measured at pH 7.4. [b] Polar surface area. [c] Efflux ratio in MDCK-MDR1 cells (10 μM incubated up to 120 min). [d] Unbound brain-to-plasma ratio measured in mice. [e] Unbound brain concentration measured in mice at C_{max} . [f] Measured in Mdr1a/1b/Bcrp knock-out mice. [g] Not tested.

P-gp liability related to the carboxylic acid function, screening of additional compounds that exhibit lower polar surface area (PSA) values than that of **1a** was performed. In this area, whilst the isoxindole compound **43** exhibited a trend toward decreased efflux, phenyl compound **48** was completely devoid of efflux in MDCK-MDR1 cells (ER value of 0.7) with high passive permeability (P_{app} value of 375 nm s^{-1}) and B_u/P_u ratio close to 1 (Table 2). This result demonstrates that in this chemical series, mitigation of efflux and improvement of in vivo brain exposure is achievable in the presence of the acidic function by decreasing the PSA or decreasing the number of hydrogen bond acceptor groups.

In conclusion, solving the structure of the (*S,R,S*)-**1a**–Keap1 complex was a breakthrough that provided experimental evidence for the true binding mode of the hit compound (*S,R,S*)-**1a**. The ligand orientation was found to differ from that of the initial docking model, which was available at the start of the project. The X-ray crystal structure helped to focus and drive the drug design process more effectively and efficiently. The design and synthesis of a further round of compounds is needed for delivering active CNS-penetrant compounds.

Acknowledgements

The authors thank Dr. T. Wayne (Evotec), Dr. C. Wilson (Evotec), C. Rospo (UCB) and her team for pharmacokinetic analysis, and R. Ward (Evotec) for chiral chromatographic purifications.

Keywords: CNS • co-crystal structures • docking • Keap1 • Nrf2 • structure–activity relationships

- [1] S. Magesh, Y. Chen, L. Hu, *Med. Res. Rev.* **2012**, *32*, 687–726.
- [2] J. Alam, D. Stewart, C. Touchard, S. Boinapally, A. M. K. Choi, J. L. Cook, *J. Biol. Chem.* **1999**, *274*, 26071–26078.
- [3] J. W. Kaspar, S. K. Niture, A. K. Jaiswal, *Free Radical Biol. Med.* **2009**, *47*, 1304–1309.
- [4] J. M. Lee, J. A. Johnson, *J. Biochem. Mol. Biol.* **2004**, *37*, 139–143.
- [5] T. Nguyen, P. J. Sherratt, C. B. Pickett, *Annu. Rev. Pharmacol. Toxicol.* **2003**, *43*, 233–260.
- [6] B. M. Hybertson, B. Gao, S. K. Bose, J. M. McCord, *Mol. Aspects Med.* **2011**, *32*, 234–246.
- [7] K. Itoh, N. Wakabayashi, Y. Katoh, T. Ishii, K. Igarashi, J. D. Engel, M. Yamamoto, *Genes Dev.* **1999**, *13*, 76–86.
- [8] A. I. Rojo, N. G. Innamorato, A. M. Martin-Moreno, M. L. De Ceballos, M. Yamamoto, A. Cuadrado, *Glia* **2010**, *58*, 588–598.
- [9] N. G. Innamorato, A. Jazwa, A. I. Rojo, C. Garcia, J. Fernandez-Ruiz, A. Grochot-Przeczek, A. Stachurska, A. Jozkowicz, J. Dulak, A. Cuadrado, *PLoS One* **2010**, *5*, e11838.
- [10] P. C. Chen, M. R. Vargas, A. K. Pani, R. J. Smeyne, D. A. Johnson, Y. W. Kan, J. A. Johnson, *Proc. Natl. Acad. Sci. USA* **2009**, *106*, 2933–2938.
- [11] C. P. Ramsey, C. A. Glass, M. B. Montgomery, K. A. Lindl, G. P. Ritson, L. A. Chia, R. L. Hamilton, C. T. Chu, K. L. Jordan-Sciutto, *J. Neuropathol. Exp. Neurol.* **2007**, *66*, 75–85.
- [12] K. Kanninen, R. Heikkinen, T. Malm, T. Rolo, S. Kuhmonen, H. Leinonen, S. Ylä-Herttua, H. Tanila, A. L. Levenon, M. Koistinaho, J. Koistinaho, *Proc. Natl. Acad. Sci. USA* **2009**, *106*, 16505–16510.
- [13] D. A. Johnson, S. Amirahmadi, C. Ward, Z. Fabry, J. A. Johnson, *Toxicol. Sci.* **2010**, *114*, 237–246.
- [14] M. R. Vargas, D. A. Johnson, D. W. Sirkis, A. Messing, J. A. Johnson, *J. Neurosci.* **2008**, *28*, 13574–13581.
- [15] M. Mazzuferi, G. Kumar, J. van Eyll, B. Danis, P. Foerch, R. M. Kaminski, *Ann. Neurol.* **2013**, *74*, 560–568.
- [16] A. J. Wilson, J. K. Kerns, J. F. Callahan, C. J. Moody, *J. Med. Chem.* **2013**, *56*, 7463–7476.
- [17] L. Hu, S. Magesh, L. Chen, L. Wang, T. A. Lewis, Y. Chen, C. Khodier, D. Inoyama, L. J. Beamer, T. J. Emge, J. Shen, J. E. Kerrigan, A. N. Kong, S. Dandapani, M. Palmer, S. L. Schreiber, B. Munoz, *Bioorg. Med. Chem. Lett.* **2013**, *23*, 3039–3043.
- [18] L. Hu, S. Magesh, L. Chen, T. Lewis, B. Munoz, L. Wang, (Rutgers University and The Broad Institute Inc.), Int. PCT Pub. No. WO2013067036 A1, **2013**.
- [19] S. C. Lo, X. Li, M. T. Henzl, L. J. Beamer, M. Hannink, *EMBO J.* **2006**, *25*, 3605–3617.
- [20] L. J. Beamer, X. Li, C. A. Bottoms, M. Hannink, *Acta Crystallogr. Sect. D* **2005**, *61*, 1335–1342.
- [21] PDB ID: 4L7B: E. Jnoff, F. Brookfield, C. Albrecht, J. J. Barker, O. Barker, E. Beaumont, S. Bromidge, M. Brooks, T. Ceska, J-P. Courade, T. Crabbe, S. Duclos, T. Fryatt, E. Jigorel, J. Kwong, Z. A. Sands, M. A. Smith.
- [22] D. Marcotte, W. Zeng, J.-C. Hus, A. McKenzie, C. Hession, P. Jin, C. Bergeron, A. Lugovskoy, I. Enyedy, H. Cuervo, D. Wang, C. Atmanene, D. Roecklin, M. Vecchi, V. Vivat, J. Kraemer, D. Winkler, V. Hong, J. Chao, M. Lukashov, L. Silvan, *Bioorg. Med. Chem. Lett.* **2013**, *21*, 4011–4019.
- [23] C. Bolm, I. Atodiresei, I. Schiffers, *Org. Synth.* **2005**, *82*, 120–125.
- [24] M. Calosso, M. Wagner, T. Gendrineau, M. Petit, C. Kadouri-Puchot, L. Dechoux, *Lett. Org. Chem.* **2007**, *4*, 4–6.
- [25] PDB ID: 4N1B: M. A. Smith, S. Duclos, E. Beaumont, J. Kwong, M. Brooks, J. J. Barker, E. Jnoff, F. Brookfield, J-P. Courade, O. Barker, T. Fryatt, C. Albrecht, S. Bromidge.
- [26] PDB ID: 4L7C: E. Jnoff, F. Brookfield, C. Albrecht, J. J. Barker, O. Barker, E. Beaumont, S. Bromidge, M. Brooks, T. Ceska, J-P. Courade, T. Crabbe, S. Duclos, T. Fryatt, E. Jigorel, J. Kwong, Z. A. Sands, M. A. Smith.
- [27] PDB ID: 4L7D: E. Jnoff, F. Brookfield, C. Albrecht, J. J. Barker, O. Barker, E. Beaumont, S. Bromidge, M. Brooks, T. Ceska, J-P. Courade, T. Crabbe, S. Duclos, T. Fryatt, E. Jigorel, J. Kwong, Z. A. Sands, M. A. Smith.

Received: December 13, 2013

Published online on February 6, 2014